

Application of entropy GRA – DoE approach in performance assessment of single slope passive solar still in various environmental conditions

Vedansh Chaturvedi, Manoj Kumar Gaur*

Department of Mechanical Engineering, Madhav Institute of Technology and Science (MITS), Gwalior (M.P.) 474005, India, emails: gmanojkumar@rediffmail.com (M.K. Gaur), vedansh.87@mitsgwalior.in (V. Chaturvedi)

Received 21 May 2022; Accepted 4 September 2022

ABSTRACT

The current research aims to implement the optimization technique to identify the best process parameters environment for single slope passive solar still located at the solar energy laboratory of MITS, Gwalior (M.P.). For this purpose, three parameters at three levels have been selected. The parameters are water depth (1, 2 and 3 cm), glass tilt angle (11°, 26° and 41°), and CuO nanoparticle concentration (0.1%, 0.15%, and 0.2% by weight). Response parameters are convective heat transfer coefficient, radiative heat transfer coefficient, evaporative heat transfer coefficient, and distilled output. The experiments were conducted as per the proposed Taguchi's L_9 orthogonal array experimental design on three sunny days of every month. K-type thermocouple used for recording all temperature inside and outside of solar still. The optimal parameter setting and most influencing parameter for all responses were investigated through signal-to-noise ratio (SNRN). Also, entropy measurement techniques are applied to find each response's entropy weightage. The grey relational analysis combines numerous responses into a single one, that is, grey relational grade. A regression equation for individual and combined responses is developed. Analysis of variance data demonstrate the percentage contribution of each parameter to solar still performance, which shows that glass tilt angle played an essential role during the study. The predicted SNRN results (16.4751, 4.15290, 23.1176, 65.7640, -0.94633 for h_r , h_c , h_{ev} , Y_c and Γ , respectively) for optimal parameter setting show the justified implementation of entropy GRA-DoE method for performance improvement in single slope passive solar still.

Keywords: Solar still parameters; Heat transfer coefficients; Distilled output; Grey relational analysis (GRA); Design of experiments (DoE); Signal-to-noise ratio (SNRN)

1. Introduction

As the world population is increasing continuously, the demand for fresh drinkable water is also increasing. Around 50 y ago, humans were not supposed to pay for drinking water, but the scenario has changed; due to drastic industrialization and pollution, normal water is very hard to drink. Due to electricity constraints, the reverse osmosis plant cannot be installed at every location. Therefore, the best eco-friendly alternative is solar still. In solar stills, saline water gets heat from sun rays inside a black painted flat basin enclosed with a sealed glass canopy. The glass surface may

be in a single slope, double slope as in traditional stills, or V-form [1]. Water desalination is necessary for many regions due to a lack of potable water with total dissolved salts less than 500 ppm [2]. Many authors report attempts to increase the performance of solar still in various ways. The distilled output of solar still is also affected by wind speed significantly [1–5]. However, wind speed's effect is sometimes less; this may be due to the seasonal change in the authors' study [6]. Solar still productivity is maximum at less water depth is reported by most of the authors [2,3,6–17]. Glass tilt angle is also a major parameter for study. The optimum tilt angle is reported by different authors 10° [18,19], 10° for summer

* Corresponding author.

and 50° for winter [20], 35° [16,21], 15° [22], 33.31° [23], 45° [24], close to latitude [25], greater than 15° [26], 30° [27], 10° double slope [28], up to 35° [29], 32.5° [30]. Ambient temperature [2,9,10], initial temperature of brine [11,31], salinity of water [32], and brine feed water temperature study were reported in the literature [33]. Reflectors show significant productivity improvement [19,34]. The modified stepped solar still with reflectors has better productivity than traditional stills [35–43]. Adding nanoparticles (cuprous oxide, aluminium oxide, nano-ferric oxide, and graphene oxide) enhanced the performance of solar stills by 10% to 25% [42,43]. Sensible heat storage material, stone bed, and glazing [44], absorptive material (black paint aluminum sheet, coal, jute cloth) [19,45], marble, pebbles, blue metal stone, basalt stone improved the productivity of solar stills [46]. Passively cooled condensers [47], modified condensation process [48], cone shape condenser [49], condenser material, and condenser area affect productivity. In contrast, the thickness of the condenser does not participate in the productivity enhancement of solar stills [50]. Effects of some other parameters are also taken into consideration by some authors, that is, thickness of glass cover [51], still coupled with flat plate collectors [52,53], sponge cube [54], alcohol distillation [55],

inclined solar water distillation (ISWD) system [56], the temperature difference between water and solar collector [57], solar still axis orientation [17], the volume of the storage tank, and the size of the heat exchanger [5], hourly radiation [5,10], insulation [10,50], basin area, external power, air blowing system and make-up water [50], parabolic trough solar collector (PTSC) [58], Fresnel lens [8]. The effects of variables are shown on daily/hourly productivity of solar still, various changes in design [59,60], Taguchi techniques [61,62], response surface methodology [63], fuzzy logic [64], artificial neural network (ANN) [65], analytical hierarchy process (AHP) for geographical preference for installation of solar still [66], flower inspired solar still developed for high productivity and low cost [67], Taguchi methods have applied for maximum solar still productivity [68]. A review of past research concluded that solar still productivity is influenced by water depth, glass tilt angle, and nanoparticles. Results are interpreted according to the locations; therefore, effects may be seen in the same parametric study.

The study for current research is carried out with water depth, glass tilt angle, and nanoparticles. A summary of previous work with these selected parameters is shown with different world locations in Table 1.

Table 1
Parametric study and their finding

Author(s)	Parameter	Finding(s)/optimum value	Location	Latitude
Tiwari [11]	Water depth	For higher initial water temperature, daily yield increases as water depth increase (Here 45°)	Delhi, India	28.7041°N
Farid and Hamad [2]	Water depth	At relatively lower water levels, the efficiency was around 50%, but it dropped to as low as 35% at deeper depths	Basrah, Iraq	30.5258°N
Singh et al. [12]	Water depth	With increasing water depth, instantaneous thermal efficiency falls	Delhi, India	28.7041°N
Toure and Meukam [6]	Water depth	With decreasing water depth, daily total production rises	Abidjan (Côte d'Ivoire)	5.3600°N
El-Sebaei [3]	Water depth	Lowest mass of water yields the most daily productivity	Tanta, Egypt	30.7865°N
Tiwari and Tiwari [13]	Water depth	Fluctuations in the value of h_c as seen at lower water depths, decrease as water depth increases	Delhi, India	28.7041°N
Phadatare and Verma [14]	Water depth	With a WD of 2 cm in the still basin, the maximum distillate output of 2.1 L/m ² -d was achieved	Lonere, India	18.1577°N
Tiwari and Tiwari [15]	Water depth	In summer and winter conditions, the daily yield of lower WD 0.02 m was 32.57% and 32.39% higher than the daily yield of higher WD 0.18 m, respectively	Delhi, India	28.7041°N
Al-Garni et al. [16]	Water depth	1 cm of WD is ideal for maximum productivity in summer and winter	Dhahran, Saudi Arabia	26.2361°N
Ajeet Kumar Rai and Kumar [17]	Water depth	Highest output is obtained at a lower depth	Allahabad, India	25.4358°N
Parekh et al. [7]	Water depth	Maximum output 2.601 L/d was found at a water depth of 3 cm	Ahmedabad, India	23.0225°N
Johnson et al. [8]	Water depth	With increasing WD, the percentage improvement in productivity rises	New Mexico	34.5199°N
Abu Abbas et al. [50]	Water depth	WD influences the water temperature of the system	Irbid, Jordan	32.5568°N
Rejeb et al. [10]	Water depth	Comparison to insulating thickness, water depth substantially impacts determining solar still efficiency	Sharjah, United Arab Emirates	25.3462°N

(Continued)

Table 1

Author(s)	Parameter	Finding(s)/optimum value	Location	Latitude
Tiwari et al. [18]	Glass tilt angle	10° in summer, inclinations should be as large as possible in winter	Delhi, India	28.7041°N
Aboul-Enein et al. [20]	Glass tilt angle	10° and 50° during the summer and winter seasons	Tanta, Egypt	30.7865°N
Elkader [21]	Glass tilt angle	35° for summer conditions	Port Said, Egypt	31.2653°N
Kumar et al. [22]	Glass tilt angle	15° for both summer and winter	Delhi, India	28.7041°N
Ali Samee et al. [23]	Glass tilt angle	33.3° for both summer and winter	Islamabad, Pakistan	33.6844°N
Hashim and Alramdhan [24]	Glass tilt angle	(Double slope) 45° for both summer and winter	Basrah City, South of Iraq	30.5258°N
Al-Garni et al. [16]	Glass tilt angle	35° for both summer and winter seasons	Eastern Saudi Arabian	23.1670°N
Khalifa [25]	Glass tilt angle	GTA should be near the latitude angle of the test location	Baghdad, Iraq	33.3152°N
Edeoja et al. [26]	Glass tilt angle	More than 15° glass tilt angle	Makurdi, Nigeria	7.7322°N
Verma [27]	Glass tilt angle	30° glass tilt angle for summer and winter	Allahabad, India	25.4358°N
El-maghlany [28]	Glass tilt angle	10° for double slope and almost equal to latitude angle	Alexandria, Egypt	31.2001°N
Begum [29]	Glass tilt angle	Up to 35° the tilt angle has a significant effect	Dhaka, Bangladesh	23.8103°N
Sahoo and Subudhi [19]	Glass tilt angle	10° is the optimum glass tilt angle	Dhenkanal, India	20.6505°N
Goshayeshi and Safaei [30]	Glass tilt angle	Optimal angle for solar still is 32.5° to the horizontal axis	Mashhad, Iran	36.2605°N
Kabeel et al. [35]	Nanoparticles	Cuprous oxide (133.64% and 93.87%) and aluminium oxide (125.0% and 88.97%) increase distilled productivity with and without the fan	Egypt	26.8206°N
Dsilva Winfred Rufuss et al. [36]	Nanoparticles	Addition of nanoparticles with PCM is superior to conventional solar stills in all aspects	Chennai, India	13.0827°N
Gupta et al. [37]	Nanoparticles	Significant improvement in distilled productivity is observed	Jabalpur, India	23.1815°N
Kabeel et al. [38]	Nanoparticles	Addition of CuO nanoparticles increased the distillate by 16% and 25%, respectively	Kafr El-Shaikh, Egypt	31.1107°N
Mahian et al. [39]	Nanoparticles	Using nanofluids as the working fluid in a heat exchanger can improve performance indices by 10%	Bangkok, Thailand	13.7563°N
Rashidi et al. [40]	Nanoparticles	Increasing the nanoparticle concentration from 0 to 5% results in a 22% increase in hourly productivity	Semnan, Iran	35.5788°N
Safaei et al. [41]	Nanoparticles	Compared to a solar still with simply PCM, the solar still containing graphene oxide/paraffin increased productivity by 25%	Vietnam	14.0583°N
Balachandran et al. [42]	Nanoparticles	Adding nano-ferric oxide in a weight proportion of 10% significantly improves yield and thermal efficiency	Tamil Nadu, India	11.1271°N
Bataineh and Abu Abbas [43]	Nanoparticles	At 0.5 cm depth of water and 0.2% nanoparticles concentration, Al ₂ O ₃ and SiO ₂ nanoparticles increased in the distilled water by 10% and 8.5%, respectively	Irbid, Jordan	32.5568°N

The hybrid technique, that is, entropy-grey relational analysis (GRA) – design of experiments (DoE), is used to optimize single slope passive solar still process parameters. This research paper presents the single and multi-response optimization for heat transfer coefficients and distilled output. Regression and ANOVA analysis were also performed to give an in-depth view of the process.

2. Experimental plan

The schematic diagram in Fig. 1 shows the solar still set-up arrangement. Three solar stills were designed and fabricated as per the Taguchi's orthogonal array experimental design.

The experimental setup is located at the solar energy lab on the MITS, Gwalior campus. The solar still experimental

setup is 1 m² in size, with all solar still pointing south. The front and back walls of solar stills are 20 and 112 cm tall, respectively. All solar stills are made of 2 mm stainless steel sheets with a zinc coating. The side and bottom of the still are insulated with a 20 mm thick thermo-col sheet. From the outside, it is supported by 20 mm thick plywood. Basin is covered by a 4 mm thick glass plate with an angle set by the level of the orthogonal array (Fig. 2).

An airtight setup is prepared with a small tank to compensate for evaporated basin water. The tray collects the droplets and transfers them to the bottle. The simple water motor is placed in the basin to stir nanoparticles as they get placed in the bottom due to high density.

The setup includes instruments for measuring the responses of various parameters at various points (Fig. 3).

K-type thermocouple with temperature indicator is used to record glass inside temperature and glass outside temperature, water temperature, vapor temperature, ambient temperature, and daily distilled output as per the parametric combination experimental run is collected in the borosilicate bottle.

The latitude of Gwalior (M.P.) city is 26.2183° N, the angle of glass is chosen close to latitude 26° [23,25], larger 41° ($\alpha + 15^\circ$) for all seasons [69], larger and smaller angle ($\alpha + 15^\circ$, $\alpha - 15^\circ$) for winter and summer season respectively [18,20]. Water depth is considered 1, 2, and 3 cm for the present study as lower water depth gives higher productivity, as reported by most of the researchers [2,3,6,12,17].

Literature reveals that adding nanoparticles increases the conduction rate of water. However, CuO nanoparticles

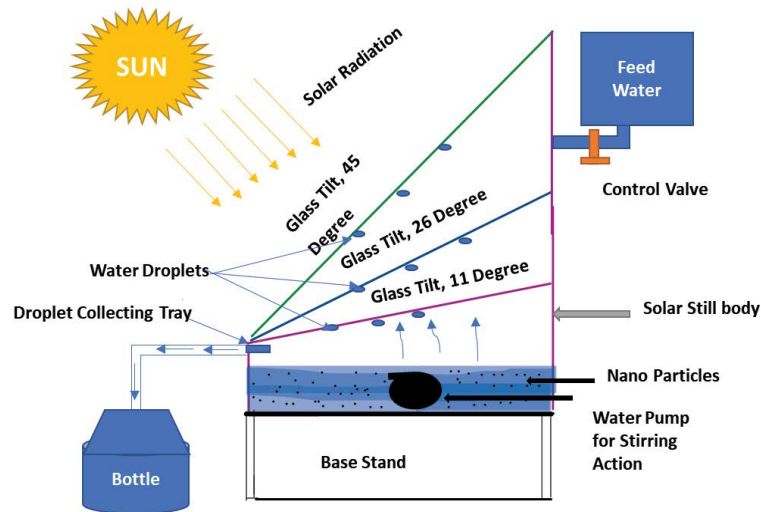


Fig. 1. Solar still set-up.

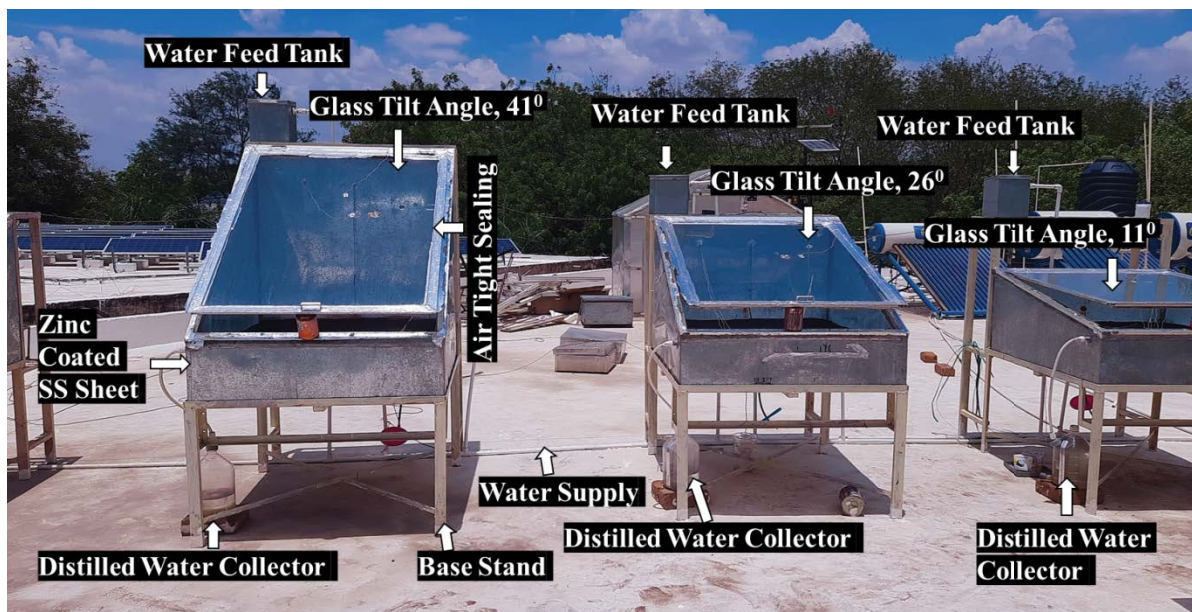


Fig. 2. Solar stills installed at MITS, Gwalior.

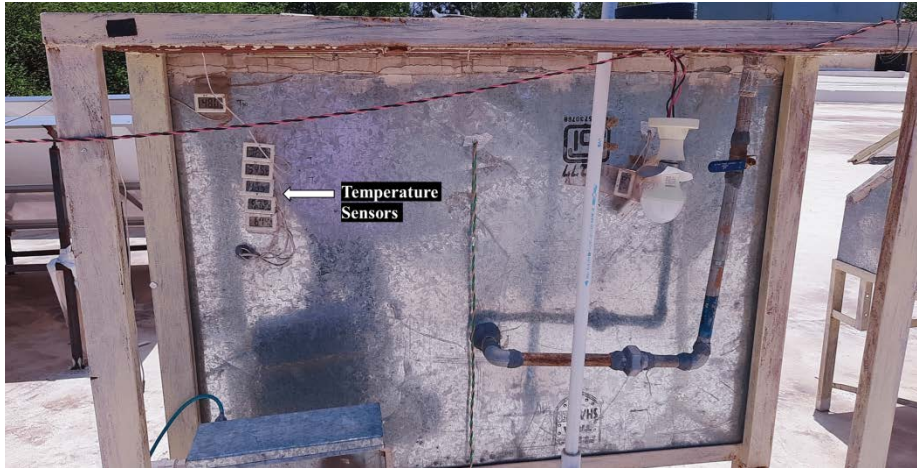


Fig. 3. Temperature indicator s.

are widely used due to their higher conductivity, density, and availability. Also, it is more effective than Al_2O_3 [35] and ZnO. According to the orthogonal array, three levels of nanoparticles percentage by weight are selected for experimental purposes (i.e., 0.1%, 0.15%, and 0.2%). The experimental design is prepared according to Taguchi's orthogonal array [70]. The variable parameters are water depth, glass tilt angle, and CuO nanoparticle concentration. The three levels are selected for the present study.

The experiments are planned according to available control parameters and their set levels shown in Table 2. Taguchi's OA (L_9) is selected for the present study. Experiments are planned for July 2020–June 2021, 3 d in a month (considered sunny days) per the experimental design. There are three solar stills setups with different parametric combination settings. Therefore, in 1 d, three experiments are scheduled to be performed during July 2020–June 2021, and a total of 108 experiments were conducted. The methodology adopted in this research is shown in Fig. 4. Table 3 shows the experimental design with coded and real values of levels corresponding to variable parameters.

2.1. Procedure adopted to prepare nanofluids

Because of their hydrophobic nature, nanoparticles are not soluble in water. Also, they settled down on the surface after some time. Therefore, the nanofluids were prepared by adopting the steps shown in Table 4.

The nanoparticles acquire hydrophilic characteristics due to the high temperature and vibration. Nanofluid may remain suspended in water for 24 h with this property.

The specific heat capacity at constant pressure (C_p) of a nanofluid [71,72] can be calculated using the following equation:

$$C_{p,nf} = \frac{[(1-\Phi)\rho_f c_{p,f} + \Phi\rho_{np}c_{p,np}]}{\Phi_f\rho_f + (1-\Phi)\rho_{np}} \quad (1)$$

where ϕ is the volume concentration of nanoparticles, and the subscripts n_f , f , and n_p represent nanofluid, base fluid, and nanoparticle, respectively.

Table 2
Variable parameters and levels

Parameters	Level		
	1	2	3
Water depth (cm)	1	2	3
Glass tilt angle (°)	11	26	41
CuO nanoparticle Concentration (weight %)	0.1	0.15	0.2

For estimating nanofluids' specific heat capacity and analyzing nanofluids' heat transfer performance [73–75], use the Eq. (2).

$$C_{p,nf} = (1-\Phi)c_{p,f} + \Phi c_{p,np} \quad (2)$$

However, it is only approximately correct for dilute suspensions when the base fluid and nanoparticles have a tiny density difference. The thermal conductivity of nanofluids [76] is derived from the following equation:

$$k_{nf} = \frac{k_p + (n-1)k_{bf} - \Phi(n-1)(k_{bf} - k_p)}{k_p + (n-1)k_{bf} + \Phi(k_{bf} - k_p)} k_{bf} \quad (3)$$

where ϕ is particle volume fraction, the subscript "bf" refers to nanofluid, and "p" refers to a particle.

Nanofluid density [77] is calculated as per the following equation:

$$\rho_{nf} = \frac{m_{nf}}{Vol_{nf}} = \frac{m_{bf} + m_p}{Vol_{bf} + Vol_p} = \frac{\rho_{bf} Vol_{bf} + \rho_p Vol_p}{Vol_{bf} + Vol_p} = (1-\Phi)\rho_{bf} + \Phi\rho_p \quad (4)$$

Indices of p , "bf" and "nf" refer to nanoparticles, base fluid, and nanofluid, respectively.

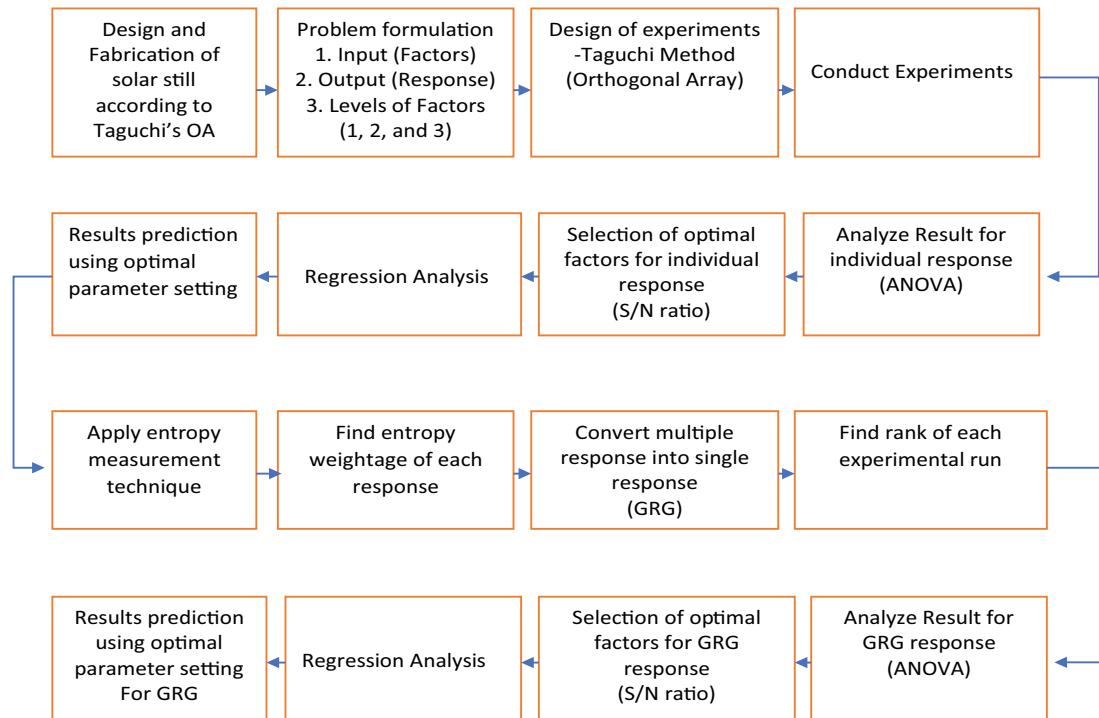


Fig. 4. Flow chart of the proposed approach.

Table 3
Taguchi's L_9 orthogonal array

Experiment No.	Coded value			Real value		
	Water depth (cm)	Glass tilt angle (°)	CuO nanoparticle concentration (weight %)	Water depth (cm)	Glass tilt angle (°)	CuO nanoparticle concentration (weight %)
1	1	1	1	1	11	0.1
2	1	2	2	1	26	0.15
3	1	3	3	1	41	0.2
4	2	1	2	2	11	0.15
5	2	2	3	2	26	0.2
6	2	3	1	2	41	0.1
7	3	1	3	3	11	0.2
8	3	2	1	3	26	0.1
9	3	3	2	3	41	0.15

The consumption of CuO nanoparticles for year-round experiments according to L_9 orthogonal array is shown in Table 5.

2.2. Uncertainty and error analysis

Type B standard uncertainty may be observed using reference [78]. The following expression may be used:

$$U(x) = \frac{\Delta x}{\sqrt{3}} = \sqrt{\frac{(\Delta x)^2}{3}} \quad (5)$$

where Δx = uncertainty level.

The other source of type B measurement uncertainty may be the invigilator's uncertainty (Δx_e); its value is estimated on the basis of the experimental skills of invigilators. Both standard deviations should be added in this case since there are two sources of type B uncertainty.

$$U(x) = \sqrt{\frac{(\Delta x)^2}{3} + \frac{(\Delta x_e)^2}{3}} \quad (6)$$

The effectiveness of solar stills is calculated using a various parameter. Glass inner temperature and glass outer temperature, water temperature, vapour temperature, ambient temperature is measured by using copper

Table 4
Procedure of nanofluids preparation





Step	Description	Image
1	Nanoparticle quantity measured as per orthogonal array design (Level 1, 2, and 3, that is, 0.1%, 0.15% and 0.2%)	
2	Nanoparticles are poured into a water filled beaker	
3	Mixture was stirred manually for 30 min	
4	Placed on the magnetic stirrer for 30 min (at 200 rpm and 40°C)	
5	In a conical flask, the mixture is poured	
6	Conical flask is placed in a small tank of ultrasonic vibrator machine to produce a sonication effect for 1 h (at 50°C)	
7	Pouring in solar still tank	

Table 5
CuO nanoparticle consumption for year-round experiments for L_o OA

Experiment No.	Water depth (cm)	CuO nanoparticle concentration (wt.%)	Area of each solar still (cm ²)	Volume of solar still for a given water depth (cm ³)	Mass of water (kg)	CuO nanoparticle required (g)
1	1	0.1	10,000	10,000	10	10
2	1	0.15	10,000	10,000	10	15
3	1	0.2	10,000	10,000	10	20
4	2	0.15	10,000	20,000	20	30
5	2	0.2	10,000	20,000	20	40
6	2	0.1	10,000	20,000	20	20
7	3	0.2	10,000	30,000	30	60
8	3	0.1	10,000	30,000	30	30
9	3	0.15	10,000	30,000	30	45
For the one-month experimental run, the CuO nanoparticle required						270
For July 2020–June 2021, the CuO nanoparticle required						3,240

constantan type thermocouple with an accuracy ($\pm 1^\circ\text{C}$), range (-50°C – 110°C) and uncertainty ($\pm 0.57\%$) is attached to digital temperature indicator.

Solar radiation was measured on glass surface level by Megger PVM210 Solarimeter with a range of 0–1,999 W/m², the accuracy of $\pm 5\%$ – 10% and uncertainty ± 0.57 W/m². Borosilicate bottle with a range of 0–5,000 mL, accuracy ± 10 mL, and uncertainty 5.77%.

2.3. Thermal analysis

The energy balance equation is written according to the following assumptions [12]:

- The solar stills are vapor leakage-proof and operate in a quasi-steady mode.
- Water absorption, heat capacity of the glass cover, and solar still insulating substance are all insignificant.
- The bottom and sides of the solar stills and the connecting pipes are entirely insulated.

The following is the energy balance for the glass cover (while neglecting its heat capacity) and the water mass in the basin: [11].

$$h_1(T_w - T_{gli}) = h_2(T_{gli} - T_a) \quad (7)$$

and

$$M_w \frac{dT_w}{dt} = \tau_1 H_s - h_1 (T_w - T_{gli}) + h_3 (T_{wb} - T_w) \quad (8)$$

The total heat transfer coefficients from the water surface to the glass and from the glass to the ambient air are provided by the formulas h_1 and h_2 .

$$h_1 = h_r + h_c + h_{ev} \quad (9)$$

where radiative heat transfer coefficient is calculated as:

$$h_r = \frac{\epsilon_{eff} \sigma \left[(T_w + 273)^4 - (T_{gli} + 273)^4 \right]}{T_w - T_{gli}} \quad (10)$$

where σ is the Stefan–Boltzmann's constant and taken as $5.67 \times 10^{-8} \text{ W/m}^2 \cdot \text{K}^4$.

$$\epsilon_{eff} = \left(\frac{1}{\epsilon_w} + \frac{1}{\epsilon_{gl}} - 1 \right)^{-1} \quad (11)$$

where the emissivity of water (ϵ_w) and the emissivity of glass (ϵ_{gl}) is considered 0.95 and 0.94, respectively [8]. The convective heat transfer (h_c) and evaporative heat transfer (h_{ev}) is derived from Eqs. (12) and (13), respectively.

Convective heat transfer coefficient:

$$h_c = 0.884 \left[T_w - T_{gli} + \frac{(P_w - P_{gli}) + (T_w + 273)}{268.9 \times 10^3 - P_w} \right]^{\frac{1}{3}} \quad (12)$$

Evaporative heat transfer coefficient:

$$h_{ev} = 16.273 \times 10^{-3} \times h_c \times \frac{P_w - P_{gli}}{T_w - T_{gli}} \quad (13)$$

and,

$$h_2 = 5.7 + 3.8v \quad (14)$$

The energy balance for basin linear is given by [11]:

$$\tau_2 H_s = h_3 (T_{wb} - T_w) + h_b (T_{wb} - T_a) \quad (15)$$

The evaporative heat flux is given by [11]:

$$q_{ev} = h_{ev} (T_w - T_{gli}) \quad (16)$$

The amount of distilled/unit area/unit time is given by [11]:

$$M_e = \frac{h_{ev} (T_w - T_{gli})}{L} \times t, \text{ kg/m}^2 \text{h} \quad (17)$$

On the sloped condensing surface, the rate of solar radiation can be calculated as [12]:

$$I_i(t) = I_b R_b + I_d R_d + (I_b - I_d) R_r \quad (18)$$

$$R_b = \frac{\cos \theta}{\cos \theta_z} \quad (19)$$

$$R_d = \frac{(1 + \cos \beta)}{2} \quad (20)$$

$$R_r = \frac{(1 - \cos \beta)}{2} \quad (21)$$

Experiments were performed according to Taguchi's L_9 OA. The study period is considered from July 2020 to June 2021, and 108 experiments are carried out. The temperature of the outer surface of the glass (T_{glo}), temperature of the inner glass surface (T_{gli}), vapor temperature (T_v), and water temperature (T_w) were recorded by digital temperature indicators (Fig. 3). The expression for temperature-dependent physical properties of vapor is given in Table 6.

Table 6
Physical properties of vapor [13]

Quantity	Expression
C_p	$999.2 + 0.1434 \times T_v + 1.101 \times 10^{-4} \times T_v^2 - 6.7581 \times 10^{-8} \times T_v^3$
ρ	$353.44 / (T_v + 273.16)$
λ	$0.0244 + 0.7673 \times 10^{-4} \times T_v$
μ	$1.718 \times 10^{-5} + 4.620 \times 10^{-8} \times T_v$
L	$3.1615 \times 10^6 \times [1 - (7.616 \times 10^{-4} \times T_v)];$ for $T_v > 70^\circ\text{C}$ $2.4935 \times 10^6 \times [1 - 9.4779 \times 10^{-4} \times T_v + 1.3132 \times 10^{-7} \times T_v^2 - 4.7974 \times 10^{-9} \times T_v^3];$ for $T_v < 70^\circ\text{C}$
P_{gli}	$\text{Exp}[25.317 - 5,144 / (T_{gli} + 273.15)]$
P_w	$\text{Exp}[25.317 - 5,144 / (T_w + 273.15)]$
β	$1 / (T_v + 273.15)$

The radiative heat transfer (h_r), convective heat transfer (h_c), and evaporative heat transfer (h_{ev}) were calculated using no. 10, 12, and 13, respectively. Also, cumulative distilled output (Y_c) is measured directly in a borosilicate bottle. The theoretically calculated cumulative distilled output (Y_c) could differ from the directly measured output due to environmental/experimental factors. Therefore, directly measured cumulative distilled output (Y_c) is taken in the present study.

The present study was performed from 12 pm to 6 am of the next day. Therefore, the positive value of (ΔT) is considered.

Fig. 5 reveals that the radiative heat transfer coefficient (h) values vary according to the different parametric combinations of water depth, glass tilt angle, and CuO nanoparticle concentration. The average value of hourly radiation from 12 pm to 6 am of the next day is used to calculate the radiative heat transfer coefficient.

The yearly value (avg. of all months) is used to analyze the parametric effect. The average value of radiative heat transfer coefficient (h_r) in Fig. 5 shows that the parametric combination water depth (WD = 3 cm, GTA = 41°, CuO = 0.15%) has a higher average radiative heat transfer coefficient.

Fig. 5 shows the season-wise effect of solar still parameter; during July 20 to Oct 20, the parametric combination (WD = 3 cm, GTA = 41°, CuO = 0.15%) gave maximum radiative heat transfer coefficient. During Nov.20–Feb.21, the parametric combination (WD = 1 cm, GTA = 41°, CuO = 0.2%) gave maximum radiation; this may be because, in winter, water takes much time to warm. Therefore, a lower depth of water increases the warming rate of water. Also, nanoparticle concentration is at a higher level which increases heat transfer.

In the case of March 21–June 21, the parametric combination (WD = 2 cm, GTA = 11°, CuO = 0.15%) gave the maximum radiative heat transfer coefficient. This may be because, in summer conditions, water depth does not affect

much as the water gets warm very early; the tilt angle is 11°, which is ($\alpha - 15^\circ$).

Fig. 6 shows the convective heat transfer coefficient (h_c) values, and overall yearly performance for the parametric setting (WD = 2 cm, GTA = 41°, CuO = 0.1%) shows a good result. However, Fig. 6 shows that in the case of seasonal performance, during July 20–Oct 20 (WD = 3 cm, GTA = 41°, CuO = 0.15%) and for winter Nov.20–Feb.21 (WD = 1 cm, GTA = 41°, CuO = 0.2%) the parametric condition for maximum convective heat transfer is same as radiative heat transfer. The maximum convective heat transfer condition for March 21–June 21 is (WD = 3 cm, GTA = 11°, CuO = 0.2%); this may be due to the good conductivity of CuO nanofluids.

Fig. 7 shows the values of evaporative heat transfer coefficient values (h_{ev}), the yearly average value is maximum for (WD = 3 cm, GTA = 41°, CuO = 0.15%), as the water depth increase the heat capacity also increase, it significantly increases the evaporation even after sunset also balanced amount of nanofluids push the heat transfer rate.

Parametric combination setting for evaporative heat transfer coefficient (h_e), during July 20–Oct.20 and Nov.20–Feb.21 the maximum rate of heat transfer found in (WD = 3 cm, GTA = 41°, CuO = 0.15%) and (WD = 1 cm, GTA = 41°, CuO = 0.2%) which is same as optimal parametric condition of h_r and h_c . Slightly change is observed for March 21–June 21 where parametric condition is (WD = 3 cm, GTA = 41°, CuO = 0.15%).

The cumulative distilled output is measured directly in the Borosilicate bottle. It is observed in Fig. 8 the yearly average value of output in mL is maximum for the parametric setting (WD = 2 cm, GTA = 11°, CuO = 0.15%),

Seasonal distilled output during July 20–Oct.20 is maximum for (WD = 3 cm, GTA = 26°, CuO = 0.1%), during Nov.20–Feb.21 the maximum output is observed for (WD = 1 cm, GTA = 41°, CuO = 0.2%). However, maximum output for the summer season March 21–June 21 is observed for (WD = 3 cm, GTA = 11°, CuO = 0.2%).

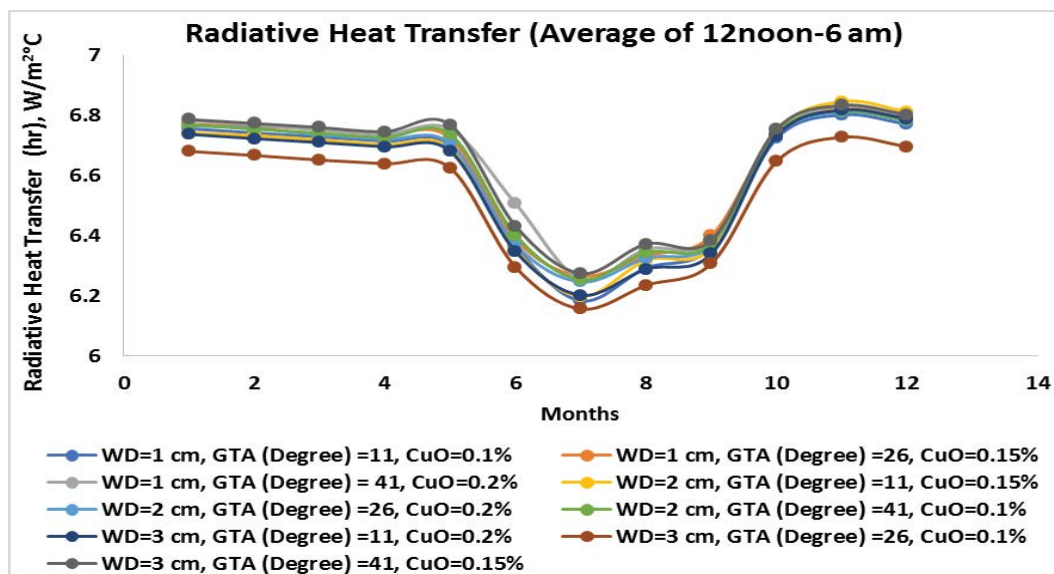


Fig. 5. Radiative heat transfer coefficient for twelve months.

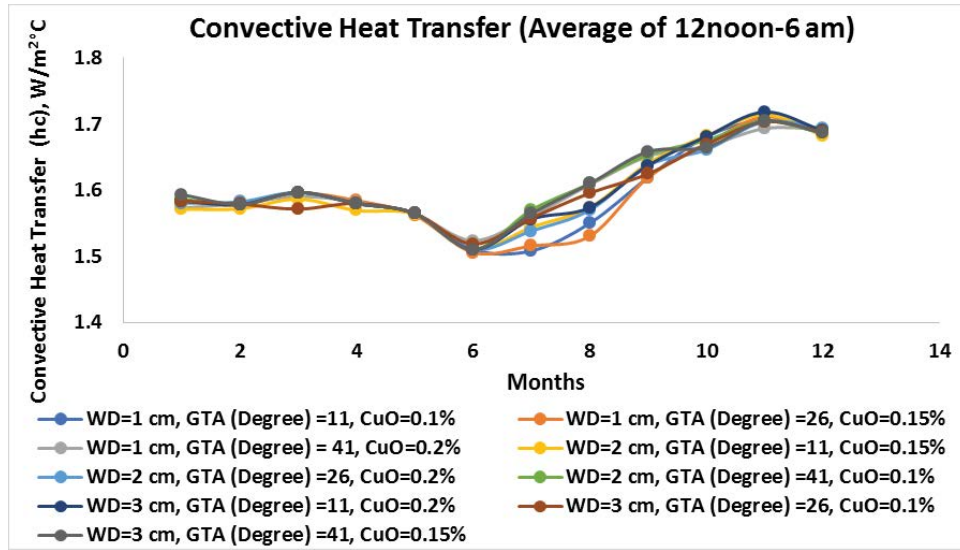


Fig. 6. Convective heat transfer coefficient for twelve months.

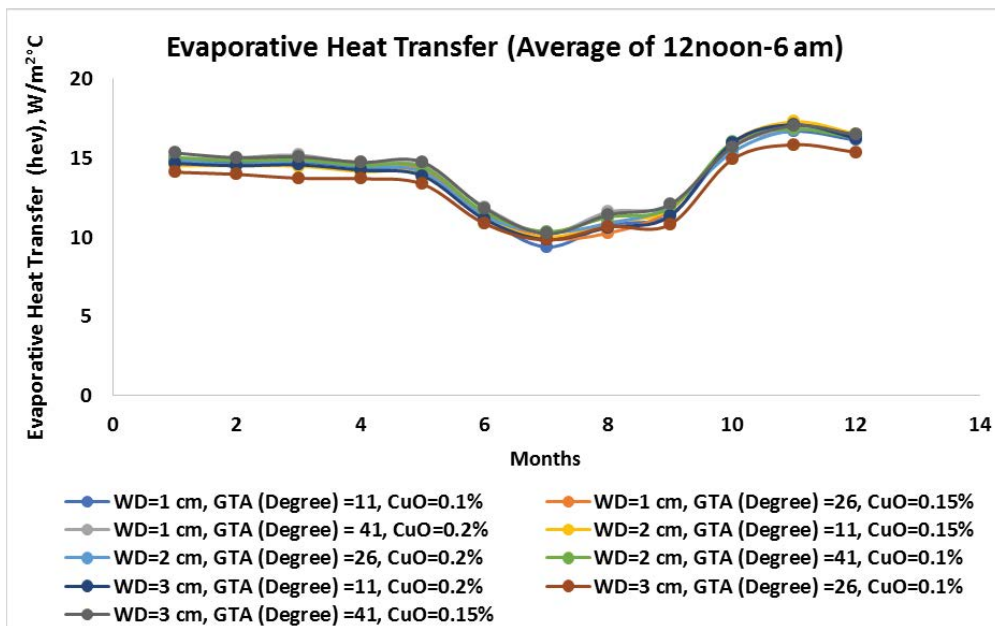


Fig. 7. Evaporative heat transfer coefficient for twelve months.

The above interpretation of h_r , h_c , h_{ev} and Y_c for optimum parametric setting reveals that parameter affects the performance of heat transfer and distilled output significantly.

2.4. Taguchi’s approach

To analyze the result of the experiments for radiative heat transfer coefficient (h_r), convective heat transfer coefficient (h_c), evaporative heat transfer coefficient (h_{ev}), and cumulative distilled output (Y_c). The signal-to-noise ratio (SNRN) was utilized.

In this respect, larger characteristics for all responses were selected to get maximum output to access the solar still performance.

The signal-to-noise ratio (SNRN) was calculated using the following Eq. (22) [70]:

$$SNRN = 10 \log \left(\frac{1}{n} \sum_{i=1}^n \frac{1}{r_i^2} \right) \tag{22}$$

where SNRN is the signal-to-noise ratio calculated based on the larger-the-better criterion, n is the total number of runs, and r_i is the response at run number i .

In addition, a quantitative investigation using variance analysis was conducted to assess the effectiveness of these parameters and determine the confidence level for each parameter to attain maximum productivity. Statistical

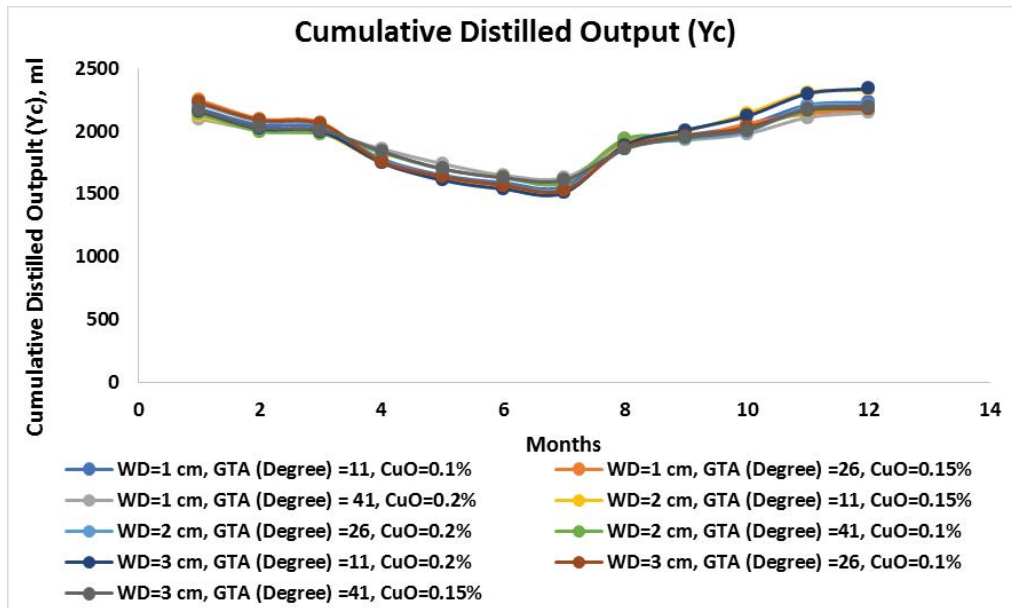


Fig. 8. Cumulative distilled output for twelve months.

analysis was also performed using the analysis of variance (ANOVA) technique to determine every parameter’s statistical significance. The *F*-test was implemented to find the most influential parameter for the solar still productivity with the highest ratio between the two variances. Variances measure deviation of data from the mean. The larger the ratio, the greater the effect of the parameter on the solar still responses [79]. The ANOVA terms and formulas have shown in Table 7.

2.5. Signal-to-noise ratio

The signal-to-noise ratio for each response is calculated using Eq. (22) and is listed in Table 8.

Regression equation for SNRN of radiative heat transfer coefficient

$$SNRN (h_r) = 16.3971 + 0.0187 \text{ water depth (cm)}_1 + 0.0074 \text{ water depth (cm)}_2 - 0.0261 \text{ water depth (cm)}_3 - 0.0133 \text{ glass tilt angle (}^\circ\text{)}_{11} - 0.0233 \text{ glass tilt angle (}^\circ\text{)}_{26} + 0.0366 \text{ glass tilt angle (}^\circ\text{)}_{41} - 0.0323 \text{ CuO concentration (\%)}_{0.10} + 0.0227 \text{ CuO concentration (\%)}_{0.15} + 0.0095 \text{ CuO concentration (\%)}_{0.20}.$$

Regression equation for SNRN of convective heat transfer coefficient

$$SNRN (h_c) = 4.09967 - 0.01919 \text{ water depth (cm)}_1 + 0.00405 \text{ water depth (cm)}_2 + 0.01515 \text{ water depth (cm)}_3 - 0.01125 \text{ glass tilt angle (}^\circ\text{)}_{11} - 0.01838 \text{ glass tilt angle (}^\circ\text{)}_{26} + 0.02963 \text{ glass tilt angle (}^\circ\text{)}_{41} - 0.00022 \text{ CuO concentration (\%)}_{0.10} - 0.00822 \text{ CuO concentration (\%)}_{0.15} + 0.00845 \text{ CuO concentration (\%)}_{0.20}.$$

Regression equation for SNRN of evaporative heat transfer coefficient

Table 7 ANOVA terms and formulas [79]

S. No.	Formula
1.	$C.F. = T^2/N$
2.	$S_T = \sum_{i=1}^{109} X_i^2 - C.F.$
3.	$S_Y = (X_{Y1}^2/N_{Y1} + X_{Y2}^2/N_{Y2} + X_{Y3}^2/N_{Y3})$
4.	$f_Y = (\text{No. of levels of parameters } Y) - 1$
5.	$f_T = (\text{Total no. of results}) - 1$
6.	$f_a = f_T + \sum f_Y$
7.	$V_Y = S_Y/f_Y$
8.	$S_e = S_T - \sum S_Y$
9.	$V_e = S_e/f_e$
10.	$F_Y = V_Y/V_e$
11.	$S_Y' = S_Y - (V_e \times f_2)$
12.	$P_z = S_Y'/S_T \times 100$
13.	$P_e = (1 - \sum P_Y) \times 100$

$$SNRN (h_{ev}) = 22.7955 + 0.0590 \text{ water depth (cm)}_1 + 0.0448 \text{ water depth (cm)}_2 - 0.1037 \text{ water depth (cm)}_3 - 0.0505 \text{ glass tilt angle (}^\circ\text{)}_{11} - 0.1248 \text{ glass tilt angle (}^\circ\text{)}_{26} + 0.1753 \text{ glass tilt angle (}^\circ\text{)}_{41} - 0.1329 \text{ CuO concentration (\%)}_{0.10} + 0.0879 \text{ CuO concentration (\%)}_{0.15} + 0.0450 \text{ CuO concentration (\%)}_{0.20}.$$

Regression equation for SNRN of cumulative distilled output

$$SNRN (Y_c) = 65.7065 - 0.01293 \text{ water depth (cm)}_1 + 0.00209 \text{ (cm)}_2 + 0.01085 \text{ water depth (cm)}_3 + 0.03583 \text{ y (}^\circ\text{)}_{11} - 0.02417 \text{ glass tilt angle (}^\circ\text{)}_{26} - 0.01166 \text{ glass tilt angle (}^\circ\text{)}_{41} - 0.00164 \text{ CuO concentration (\%)}_{0.10} + 0.01084 \text{ CuO concentration (\%)}_{0.15} - 0.00920 \text{ CuO concentration (\%)}_{0.20}.$$

Taguchi’s approach determines the signal-to-noise ratio (SNRN) for all responses; larger is better characteristics are considered for the study. The SNRN for all individual responses is calculated using Eq. (22) and shown in Table 8.

Optimal process parameter setting was found in the main effect plot for SN ratios. Fig. 9 shows that (WD = 1 cm, GTA = 41°, CuO = 0.15%) is the optimal condition for radiative heat transfer coefficient.

Similarly, Fig. 10 shows the optimal condition for convective heat transfer coefficient (WD = 3 cm, GTA = 41°,

CuO = 0.20%), Fig. 11 shows the optimal condition for evaporative heat transfer coefficient (WD = 1 cm, GTA = 41°, CuO = 0.15%).

The SN plot of the yearly average distilled output in Fig. 12 shows that (WD = 3 cm, GTA = 11°, CuO = 0.15%) is the optimized process parameters condition for the maximum distilled output.

In statistics, variance analysis is a term that is used to determine the effect of process parameters on responses in percentage. ANOVA for responses is shown in Tables 9–12,

Table 8
SN ratio of each response

Ex. No.	Yearly avg. radiative heat transfer	SNRN (h_r)	Yearly avg. convective heat transfer	SNRN (h_c)	Yearly avg. evaporative heat transfer	SNRN (h_{ev})	Yearly avg. cumulative distilled output	SNRN (Y_c)
1	6.59451	16.3836	1.59684	4.06523	13.6870	22.7262	1,935.00	65.7336
2	6.62471	16.4233	1.59503	4.05536	13.8900	22.8541	1,923.33	65.6811
3	6.63782	16.4405	1.60710	4.12085	14.0982	22.9833	1,920.00	65.6660
4	6.60126	16.3925	1.60076	4.08653	13.7819	22.7862	1,938.33	65.7486
5	6.61012	16.4042	1.60140	4.09001	13.8287	22.8156	1,923.33	65.6811
6	6.61981	16.4169	1.60965	4.13461	13.9945	22.9192	1,926.67	65.6961
7	6.58822	16.3754	1.60574	4.11349	13.6818	22.7228	1,937.50	65.7448
8	6.52687	16.2941	1.60297	4.09851	13.0957	22.3426	1,924.17	65.6849
9	6.64029	16.4437	1.60925	4.13245	14.1415	23.0099	1,932.50	65.7224

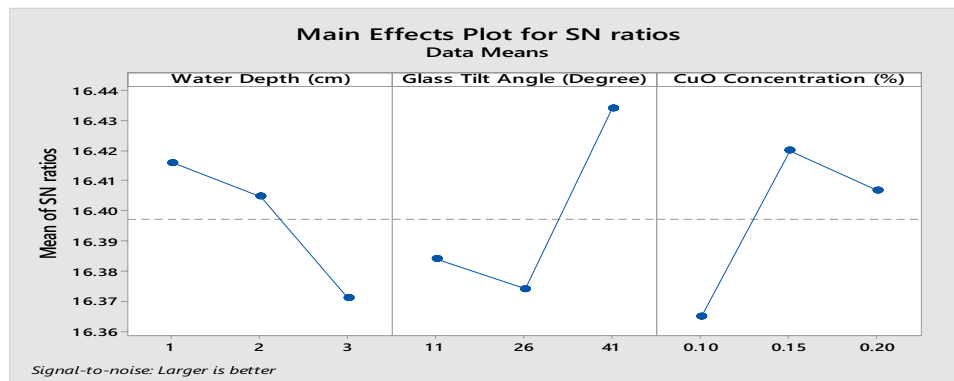


Fig. 9. SN ratio of h_r .

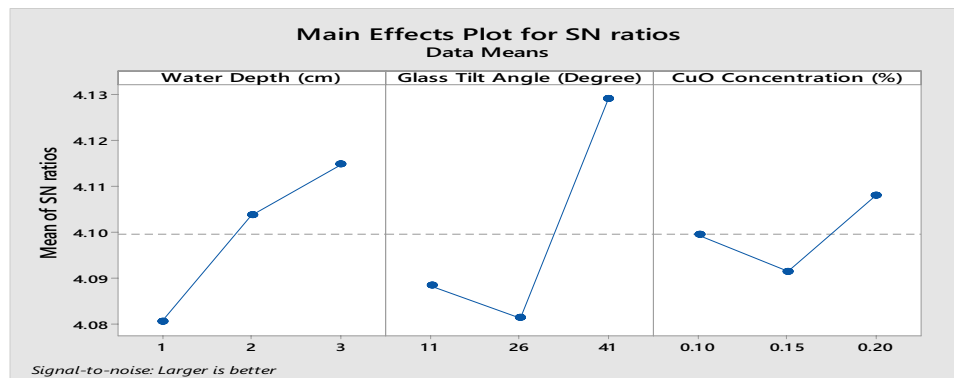


Fig. 10. SN ratio of h_c .

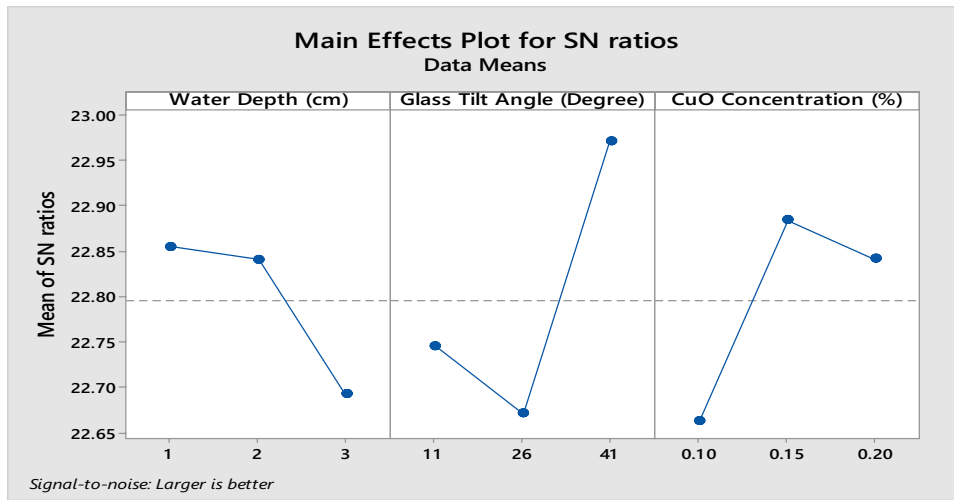


Fig. 11. SN ratio of h_{ev} .

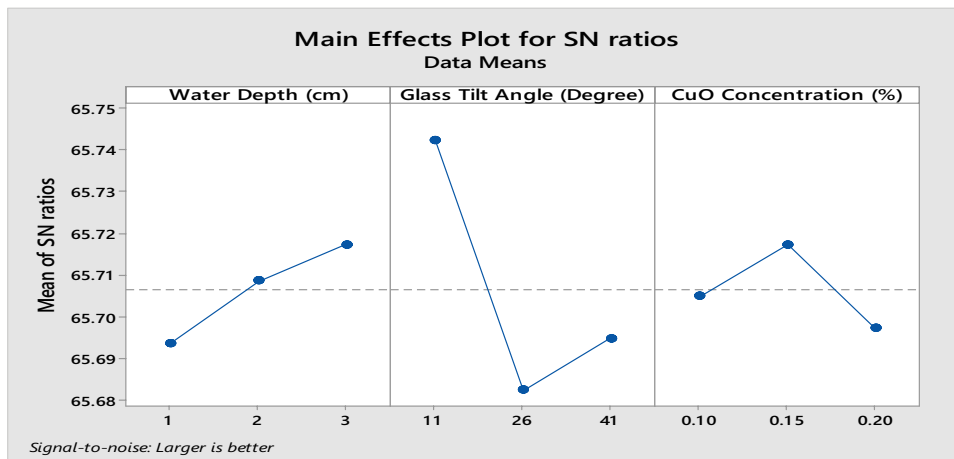


Fig. 12. SN ratio of Y_c .

Table 9
ANOVA for radiative heat transfer coefficient

Source	df	Seq. SS	Contribution	Adj. SS	Adj. MS	F-value	P-value
Water depth (cm)	2	0.003253	19.74%	0.003253	0.001626	1.54	0.393
Glass tilt angle (°)	2	0.006169	37.44%	0.006169	0.003084	2.92	0.255
CuO concentration (%)	2	0.004944	30.01%	0.004944	0.002472	2.34	0.299
Error	2	0.002109	12.80%	0.002109	0.001055		
Total	8	0.016476	100.00%				

which shows the percentage contribution of process parameters in response study. Glass tilt angle showing the highest percentage contribution in all ANOVA studies. Table 9 shows the ANOVA for h_r and found that GTA contributes 37.44%, CuO 30.01%, and WD 19.74%. Table 10 for h_c shows that GTA contributes 63.41%, CuO 6.56%, and WD 29.01%. Table 11 for h_{ev} shows that GTA contributes 46.41%, CuO 26.05%, and WD 15.44%. Table 12 for the yearly average distilled output (Y_c) shows that GTA contributes 77.74%, CuO 7.94%, and WD 11.22%.

2.6. Grey relational analysis

The number of experimental runs as per Taguchi's OA design is m , and the number of quality characteristics is n . The following series of expressions can be used to express the experimental results: [80].

$$X_1, X_2, X_3, \dots, X_r, \dots, X_m$$

$$\text{where } X_1 = \{X_1(1), X_1(2), \dots, X_1(k), \dots, X_1(n)\};$$

Table 10
ANOVA for convective heat transfer coefficient

Source	df	Seq. SS	Contribution	Adj. SS	Adj. MS	F-value	P-value
Water depth (cm)	2	0.001843	29.01%	0.001843	0.000921	28.32	0.034
Glass tilt angle (°)	2	0.004027	63.41%	0.004027	0.002014	61.91	0.016
CuO concentration (%)	2	0.000417	6.56%	0.000417	0.000208	6.41	0.135
Error	2	0.000065	1.02%	0.000065	0.000033		
Total	8	0.006352	100.00%				

Table 11
ANOVA for evaporative heat transfer coefficient

Source	df	Seq. SS	Contribution	Adj. SS	Adj. MS	F-value	P-value
Water depth (cm)	2	0.04874	15.44%	0.04874	0.02437	1.28	0.439
Glass tilt angle (°)	2	0.14649	46.41%	0.14649	0.07324	3.83	0.207
CuO concentration (%)	2	0.08222	26.05%	0.08222	0.04111	2.15	0.317
Error	2	0.03820	12.10%	0.03820	0.01910		
Total	8	0.31565	100.00%				

Table 12
ANOVA for cumulative distilled output

Source	df	Seq. SS	Contribution	Adj. SS	Adj. MS	F-value	P-value
Water depth (cm)	2	0.000868	11.22%	0.000868	0.000434	3.62	0.216
Glass tilt angle (°)	2	0.006011	77.74%	0.006011	0.003006	25.10	0.038
CuO concentration (%)	2	0.000614	7.94%	0.000614	0.000307	2.56	0.281
Error	2	0.000239	3.10%	0.000239	0.000120		
Total	8	0.007733	100.00%				

$X_i = \{X_i(1), X_i(2), \dots, X_i(k), \dots, X_i(n)\};$
 $X_m = \{X_m(1), X_m(2), \dots, X_m(k), \dots, X_m(n)\};$
 X_i represents the result of i th experimental and is called the comparative sequence in grey relational analysis.

Let, X_0 be the reference sequence:

Let, $X_0 = \{X_0(1), X_0(2), \dots, X_0(k), \dots, X_0(n)\}.$

The optimal value of the related quality feature is the value of the components in the reference sequence. X_0 and X_i both include n elements and $X_0(k)$ and $X_i(k)$ represent the numeric value of k th element in the reference sequence and the comparative sequence, respectively $k = 1, 2, \dots, n$. The proposed parameter optimization approaches are thoroughly illustrated in the following sections.

Step 1: Normalization of the quality characteristics

When the range of a series is too broad, or the optimal value of a quality trait is too high, some elements are neglected. The initial response data must be normalised to eliminate this effect. There are three methods of data normalisation depending on whether we need the LB (lower is better), NB (nominal is best), or HB (higher the

better). Grey relational generation is the term for this process. The following equations are used to normalise the data.

(a) LB (lower-the-better)

$$X_i^*(k) = \frac{\min X_i(k)}{X_i(k)} \quad (23)$$

(b) HB (higher-the-better)

$$X_i^*(k) = \frac{X_i(k)}{\max X_i(k)} \quad (24)$$

(c) NB (nominal-the-best)

$$X_i^*(k) = \frac{\min\{X_i(k), X_{ob}(K)\}}{\max\{X_i(k), X_{ob}(K)\}} \quad (25)$$

where $i = 1, 2, \dots, m; k = 1, 2, \dots, n$.

$X_i^*(k)$ is the normalized data of the k th element in the i th sequence.

$X_{0b}(k)$ is the required value of the k th quality characteristic. After data normalization, the value of $X_i^*(k)$ will be between 0 and 1. The series X_i^* , $i = 1, 2, 3, \dots, m$ can be viewed as the comparative sequence used in the grey relational analysis.

Step 2: Individual grey relational grades calculation

To evaluate the grey relational coefficient between $X_0(k)$ and $X_i(k)$, use the following equation.

$$r_{0,i}(k) = \frac{\Delta_{\min} + \xi\Delta_{\max}}{\Delta_{0,i} + \xi\Delta_{\max}}, \quad i = 1, 2, \dots, m; \quad k = 1, 2, \dots, n \quad (26)$$

where $r_{0,i}(k)$ is the relative difference of k th element between sequence X_i and the comparative sequence X_0 (also called grey relational grade), and $\Delta_{0,i}(k)$ is the absolute value of the difference between $X_0(k)$ and $X_i(k)$.

where $\Delta_{0i} = \|X_0(k) - X_i(k)\|$ = difference of the absolute value $X_0(k)$ and $X_i(k)$; φ is the distinguishing coefficient $0 \leq \varphi \leq 1$; $\Delta_{\min} = \forall j^{\min} \in i \forall k^{\min} \|X_0(k) - X_i(k)\|$ = the smallest value of Δ_{0i} ; and $\Delta_{\max} = \forall j^{\max} \in i \forall k^{\max} \|X_0(k) - X_i(k)\|$ = largest value of Δ_{0i} . ξ is known as the distinguishing coefficient, and its value ranges from 0 to 1. It is usually set at 0.5 [80].

Step 3: Weight of each quality attribute is calculated using the entropy approach

Entropy is a measure of how chaotic a system is in information theory. When entropy is applied to a weight measurement, a big entropy indicates that the attribute has a wide range of responses, implying that the characteristic has more meaningful effects. In grey relational analysis, the entropy measurement approach has recently been utilised to determine the weights. The mapping function $f_i: [0,1] \rightarrow [0,1]$ used in entropy should be satisfied three conditions: (1) $f_i(0) = 0$; (2) $f_i(x) = f_i(1-x)$ and (3) $f_i(x)$ is monotonic increasing in the range $x \in (0,0.5)$. Thus, the following function $w_e(x)$ may be used as the mapping function in entropy measure.

$$w_e(x) = x \cdot e^{(1-x)} + (1-x) \cdot e^{-x} - 1 \quad (27)$$

The highest value of this function occurs at $x = 0.5$, and the value is $e^{0.5} - 1 = 0.6487$. In order to get the mapping result in the range $[0,1]$ defined new entropy [81]:

$$W \equiv \frac{1}{(e^{0.5} - 1)} \sum_{i=1}^m w_e(x_i) \quad (28)$$

Assume that there is a sequence $\epsilon_i = \{r_i(1), r_i(2), \dots, r_i(n)\}$. Where, $r_i(j)$ is the grey relational coefficient. Note that $i = 1, 2, \dots, m; j = 1, 2, \dots, n$.

The following are the processes for calculating weight: [81].

- (a) Computation of the D_j (sum of the grey relational coefficient in all sequences for each quality characteristic)

$$D_j = \sum_{i=1}^m r_i(j), \quad j = 1, 2, \dots, n \quad (29)$$

- (b) Computation of the normalized coefficient

$$k = \frac{1}{(e^{0.5} - 1) \times m} = \frac{1}{0.6487 \times m} \quad (30)$$

- (c) Computation of the entropy of each quality characteristics

$$e_j = k \sum_{i=1}^m w_e \left(\frac{r_i(j)}{D_j} \right), \quad j = 1, 2, \dots, n \quad (31)$$

where $w_e(x) = x \cdot e^{(1-x)} + (1-x) \cdot e^{-x} - 1$

- (d) Computation of the sum of entropy

$$E = \sum_{j=1}^n e_j \quad (32)$$

- (e) Computation of the weight of each response parameter:

$$w_j = \frac{1}{n - E} \cdot \frac{[1 - e_j]}{\sum_{j=1}^n \frac{1}{n - E} \cdot [1 - e_j]} \quad (33)$$

where $j = 1, 2, \dots, n$.

Step 4: Computation of the overall grey relational grade

After the grey relational coefficient has been calculated, the grey relational grade is determined:

$$\Gamma_{0,i} = \sum_{k=1}^n w_k r_{0,i}(k), \quad i = 1, 2, \dots, m \quad (34)$$

Table 13 shows the yearly average value of measured responses, data normalization for higher-is-better characteristics performed on the response values using Eq. (24) and given in Table 14.

Table 15 represents individual and overall grey relational grades for each experimental run calculated using Eq. (26) and (34). Experiment no. 9 has rank 1, which shows a good combination for maximum output of all responses. However, experiment no. 8 at no. 9 indicates that this parametric combination is not effective for all the responses.

Regression equation for SNRN of grey relational grade

SNRN (Γ) = $-4.175 - 0.214$ water depth (cm)_1 + 0.269 water depth (cm)_2 - 0.055 water depth (cm)_3 + 0.007 glass tilt angle ($^\circ$)_11 - 2.097 glass tilt angle ($^\circ$)_26 + 2.091 glass tilt angle ($^\circ$)_41 - 1.127 CuO concentration (%)_0.10 + 0.869 CuO concentration (%)_0.15 + 0.258 CuO concentration (%)_0.20.

Table 16 represents the signal-to-noise ratio (SNRN) for a grey relational grade. The optimal parameter setting is

Table 13
Yearly average value of measured responses for L₉ OA experiments

Ex. no.	Water depth (cm)	Glass tilt angle (°)	CuO concentration (weight %)	h_c (W/m ² .°C)	h_{ev} (W/m ² .°C)	h_r (W/m ² .°C)	Y_c (mL)
1	1	11	0.1	1.5968	13.6870	6.5945	1,935.0000
2	1	26	0.15	1.5950	13.8900	6.6247	1,923.3333
3	1	41	0.2	1.6071	14.0982	6.6378	1,920.0000
4	2	11	0.15	1.6008	13.7819	6.6013	1,938.3333
5	2	26	0.2	1.6014	13.8287	6.6101	1,923.3333
6	2	41	0.1	1.6096	13.9945	6.6198	1,926.6667
7	3	11	0.2	1.6057	13.6818	6.5882	1,937.5000
8	3	26	0.1	1.6030	13.0957	6.5269	1,924.1667
9	3	41	0.15	1.6092	14.1415	6.6403	1,932.5000

Table 14
Data normalization

	h_c	h_{ev}	h_r	Y_c
Ideal condition	1	1	1	1
Ex. No. 1	0.9921	0.9679	0.9931	0.9983
Ex. No. 2	0.9909	0.9822	0.9977	0.9923
Ex. No. 3	0.9984	0.9969	0.9996	0.9905
Ex. No. 4	0.9945	0.9746	0.9941	1.0000
Ex. No. 5	0.9949	0.9779	0.9955	0.9923
Ex. No. 6	1.0000	0.9896	0.9969	0.9940
Ex. No. 7	0.9976	0.9675	0.9922	0.9996
Ex. No. 8	0.9959	0.9261	0.9829	0.9927
Ex. No. 9	0.9998	1.0000	1.0000	0.9970

Table 16
SN ratio of GRG

Water depth (cm)	Glass tilt angle (°)	CuO concentration (%)	GRG	SNRN (T)
1	11	0.10	0.546884	-5.24209
1	26	0.15	0.543005	-5.30392
1	41	0.20	0.739511	-2.62111
2	11	0.15	0.659844	-3.61117
2	26	0.20	0.532245	-5.47776
2	41	0.10	0.738769	-2.62983
3	11	0.20	0.656741	-3.65212
3	26	0.10	0.396483	-8.03551
3	41	0.15	0.891003	-1.00242

Table 15
Individual and overall, GRG

Individual grey relational grade				Overall grey relational grade	Rank
h_c	h_{ev}	h_r	Y_c	Γ	
0.091309	0.133277	0.137941	0.184356	0.546884	6
0.083749	0.168235	0.195515	0.095505	0.543005	7
0.186636	0.230139	0.23879	0.083946	0.739511	2
0.113465	0.147617	0.147662	0.2511	0.659844	4
0.11815	0.155881	0.162709	0.095505	0.532245	8
0.2504	0.194492	0.18312	0.110756	0.738769	3
0.163945	0.132565	0.129971	0.23026	0.656741	5
0.13142	0.08303	0.083123	0.09891	0.396483	9
0.23889	0.2492	0.2492	0.153713	0.891003	1

Table 17
ANOVA for GRG

Source	df	Seq. SS	Contribution	Adj. SS	Adj. MS	F-value	P-value
Water depth (cm)	2	0.3632	1.05%	0.3632	0.1816	0.24	0.807
Glass tilt angle (°)	2	26.3085	76.32%	26.3085	13.1543	17.29	0.055
CuO concentration (%)	2	6.2797	18.22%	6.2797	3.1398	4.13	0.195
Error	2	1.5212	4.41%	1.5212	0.7606		
Total	8	34.4726	100.00%				

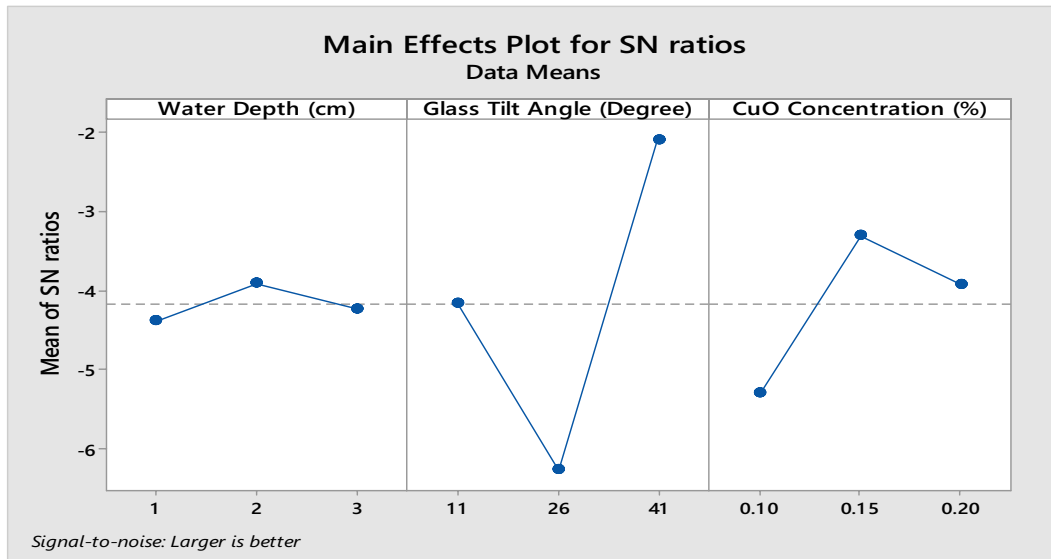


Fig. 13. SN ratio of GRG (Γ).

Table 18
Predicted SNRN for optimal parameter setting

Response	Optimal parameter setting	Predicted SNRN
h_r	WD = 1 cm, GTA = 41°, CuO = 0.15%	16.4751
h_c	WD = 3 cm, GTA = 41°, CuO = 0.20%	4.15290
h_{ev}	WD = 1 cm, GTA = 41°, CuO = 0.15%	23.1176
Y_c	WD = 3 cm, GTA = 11°, CuO = 0.15%	65.7640
Γ	WD = 2 cm, GTA = 41°, CuO = 0.15%	-0.94633

shown in Fig. 13, which shows that (WD = 2 cm, GTA = 41°, CuO = 0.15%) is the best process parameters setting for multi-response optimization.

Table 17 shows that glass tilt angle contributes 76.32%, CuO concentration 18.22%, and WD 1.05% in multi-response optimization. Again, the glass tilt angle has the most significant parameter, which shows that even in multi-response optimization, the glass tilt angle is similarly important as it is in individual response; this may be due to that water depth which is considered for this study do not have much difference in depth. Therefore, the effect of WD is negligible in the present study. However, the other two factors were essential in the present parametric study. The water depth effect may be seen if the depth difference is high.

3. Conclusions

The parametric analysis is carried out in this research to discover the ideal process environment for single slope passive solar still. To support the investigation, the following observations were made.

- The best process parameters combination for radiative and evaporative heat transfer coefficient is (WD = 1 cm, GTA = 41°, CuO = 0.15%). The predicted SNRN value is 16.4751 for radiative heat transfer coefficient and 23.1176 for evaporative heat transfer coefficient.

- The best process parameters combination predicted for convective heat transfer coefficient is (WD = 3 cm, GTA = 41°, CuO = 0.20%), and the predicted SNRN value is 4.15290.
- The best process parameters combination for cumulative distilled output is (WD = 3 cm, GTA = 11°, CuO = 0.15%), and the predicted SNRN value is 65.7640.
- A single response is created from multiple responses, that is, grey relational grade (GRG), using entropy measurement technique, which is shown in Table 15.
- The optimal combination of process parameters for grey relational grade (GRG) is (WD = 2 cm, GTA = 41°, CuO = 0.15%), and the predicted SNRN value is -0.94633.
- Glass tilt angles have the highest percentage contribution in single slope passive solar still performance for individual and multi-response optimization.
- Table 18 shows the predicted SNRN values for given responses. It indicates good agreement as the predicted SNRN value is more than the SNRN of experimental values which is shown in Table 18.

Symbols

WD	—	Water depth, cm
GTA	—	Glass tilt angle (°)
T_w	—	Temperature of water, °C
T_v	—	Temperature of water vapor, °C
T_{gli}	—	Temperature of glass inner surface, °C
T_{glo}	—	Temperature of glass outer surface, °C
T_a	—	Temperature of ambient air, °C
T_{wb}	—	Temperature of water basin, °C
P_w	—	Partial saturated vapor pressure at water temperature, N/m ²
P_{gli}	—	Partial saturated vapor pressure at glass inner cover temperature, N/m ²
C_p	—	Specific heat
ρ	—	Density
λ	—	Thermal conductivity
μ	—	Viscosity

β	—	Expansion factor
h_r	—	Radiative heat transfer coefficient, $W/m^2 \cdot ^\circ C$
h_c	—	Convective heat transfer coefficient, $W/m^2 \cdot ^\circ C$
h_{ev}	—	Evaporative heat transfer coefficient, $W/m^2 \cdot ^\circ C$
Y_c	—	Cumulative distilled output, mL
$I_i(t)$	—	Solar radiation at time (t), W/m^2
I_b	—	Intensity of beam radiation, W/m^2
I_d	—	Intensity of diffuse radiation, W/m^2
R_b	—	Conversion or geometric factors for beam radiation
R_d	—	Conversion or geometric factors for diffuse radiation
R_r	—	Conversion or geometric factors for diffuse radiation reflected for the ground and surroundings
t	—	Time, h
SNRN	—	Signal-to-noise ratio
ANOVA	—	Analysis of variance
C.F.	—	Correction factor
T	—	Total of all result
N	—	Total no. of experiments
X_{Y1}, X_{Y2}, X_{Y3}	—	Values of a result of each level (i.e., 1, 2, 3) of parameters Y
X_i	—	Value of result of each experiment ($i = 1$ to 9)
N_{Y1}, N_{Y2}, N_{Y3}	—	Repeating no. of each level (1, 2, 3) of parameter Y
S_Y	—	Sum of the squares of due to parameters Y ($Y = A, B, C$)
S_T	—	Total sum of squares to total variance
S_e	—	Sum of square of error terms
f_Y	—	Degree of freedom of parameter Y
f_T	—	Total degree of freedom
f_e	—	Error of degree of freedom
V_Y	—	Variance of parameter Y
V_e	—	Error of variance
F_Y	—	F -ratio of parameter of Y
$S_{Y'}$	—	Pure sum of square
P_Y	—	Percentage contribution of parameter Y
P_e	—	Percentage contribution of error term

Greeks

α	—	Latitude, ($^\circ$)
Γ	—	Grey relational grade
σ	—	Stefan-Boltzmann's constant, $5.67 \times 10^{-8} W/m^2 \cdot K^4$
ϵ_{eff}	—	Effective emissivity between water basin and glass cover
ϵ_w	—	Emissivity of water
ϵ_{gl}	—	Emissivity of glass
v	—	Wind velocity, m/s

Subscripts

w	—	Water
v	—	Vapor
gl	—	Glass

gli	—	Glass inner surface
glo	—	Glass outer surface
a	—	Ambient
wb	—	Water basin
r	—	Radiative
c	—	Convective
ev	—	Evaporative
b	—	Beam
d	—	Diffuse
Y	—	Parameter
T	—	Total
e	—	Error

Acknowledgments

The author is thankful to the Dept. of Mechanical Engineering, MITS Gwalior, who provided Solar Lab for this work.

References

- [1] H.P. Garg, H.S. Mann, Effect of climatic, operational and design parameters on the year round performance of single-sloped and double-sloped solar still under Indian arid zone conditions, *Sol. Energy*, 18 (1976) 159–163.
- [2] M. Farid, F. Hamad, Performance of a single-basin solar still, *Renewable Energy*, 3 (1993) 75–83.
- [3] A.A. El-Sebaii, Effect of wind speed on some designs of solar stills, *Energy Convers. Manage.*, 41 (2000) 523–538.
- [4] A.A. El-Sebaii, Effect of wind speed on active and passive solar stills, *Energy Convers. Manage.*, 45 (2004) 1187–1204.
- [5] N. Smakdji, A. Kaabi, B. Lips, Optimization and modeling of a solar still with heat storage, *Desal. Water Treat.*, 52 (2014) 1761–1769.
- [6] S. Toure, P. Meukam, A numerical model and experimental investigation for a solar still in climatic conditions in Abidjan (Côte d'Ivoire), *Renewable Energy*, 11 (1997) 319–330.
- [7] W. Parekh, M. Patel, N. Patel, J. Prajapati, M. Patel, Optimization of water output by experimental analysis on passive solar still, *IOP Conf. Ser.: Mater. Sci. Eng.*, 310 (2018) 012058.
- [8] A. Johnson, L. Mu, Y.H. Park, D.J. Valles, H. Wang, P. Xu, K. Kota, S. Kuravi, A thermal model for predicting the performance of a solar still with fresnel lens, *Water (Switzerland)*, 11 (2019) 1860, doi: 10.3390/w11091860.
- [9] M.O.A. Abbas, M.Y. Al-Abed Allah, Q.N. Al-Oweiti, Optimization analysis of active solar still using design of experiment method, *Drinking Water Eng. Sci. Discuss.*, (2020), doi: 10.5194/dwes-2020-22.
- [10] O. Rejeb, M.S. Yousef, C. Ghenai, H. Hassan, M. Bettayeb, Investigation of a solar still behaviour using response surface methodology, *Case Stud. Therm. Eng.*, 24 (2021) 100816, doi: 10.1016/j.csite.2020.100816.
- [11] G.N. Tiwari, Madhuri, Effect of water depth on daily yield of the still, *Desalination*, 61 (1987) 67–75.
- [12] A.K. Singh, G.N. Tiwari, P.B. Sharma, E. Khan, Optimization of orientation for higher yield of solar still for a given location, *Energy Convers. Manage.*, 36 (1995) 175–181.
- [13] A.K. Tiwari, G.N. Tiwari, Effect of water depths on heat and mass transfer in a passive solar still: in summer climatic condition, *Desalination*, 195 (2006) 78–94.
- [14] M.K. Phadatare, S.K. Verma, Influence of water depth on internal heat and mass transfer in a plastic solar still, *Desalination*, 217 (2007) 267–275.
- [15] A.K. Tiwari, G.N. Tiwari, Thermal modeling based on solar fraction and experimental study of the annual and seasonal performance of a single slope passive solar still: the effect of water depths, *Desalination*, 207 (2007) 184–204.
- [16] A.Z. Al-Garni, A.H. Kassem, F. Saeed, F. Ahmed, Effect of glass slope angle and water depth on productivity of double slope solar still, *J. Sci. Ind. Res. (India)*, 70 (2011) 884–890.

- [17] V.K.V. Ajeet Kumar Rai, A. Kumar, Effect of water depth and still orientation on productivity of passive solar still, *Int. J. Mech. Eng. Technol.*, 5 (2014) 36–43.
- [18] G.N. Tiwari, J.M. Thomas, E. Khan, Optimisation of glass cover inclination for maximum yield in a solar still, *Heat Recovery Syst. CHP*, 14 (1994) 447–455.
- [19] B.B. Sahoo, C. Subudhi, Performance enhancement of solar still by using reflectors-jute cloth-improved glass angle, *J. Eng. Res.*, 16 (2019) 1–10.
- [20] S. Aboul-Enein, A.A. El-Sebaei, E. El-Bialy, Investigation of a single-basin solar still with deep basins, *Renewable Energy*, 14 (1998) 299–305.
- [21] M.A. Elkader, An Investigation of the parameters involved in simple solar still with inclined yute, *Renewable Energy*, 14 (1998) 333–338.
- [22] S. Kumar, G.N. Tiwari, H.N. Singh, Annual performance of an active solar distillation system, *Desalination*, 127 (2000) 79–88.
- [23] M. Ali Samee, U.K. Mirza, T. Majeed, N. Ahmad, Design and performance of a simple single basin solar still, *Renewable Sustainable Energy Rev.*, 11 (2007) 543–549.
- [24] A.Y. Hashim, W.A.T. Alramdhan, An attempt to solar still productivity optimization; solar still shape, glass cover inclination and inner surface area of a single basin solar still, *optimization, Basrah J. Sci.*, 28 (2010) 39–48.
- [25] A.J.N. Khalifa, On the effect of cover tilt angle of the simple solar still on its productivity in different seasons and latitudes, *Energy Convers. Manage.*, 52 (2011) 431–436.
- [26] F. Edeoja, A. Okibe, Unom, Investigation of the effect of angle of cover inclination on the yield of a single basin solar still under Makurdi climate, *Energy Procedia*, 14 (2013) 131–138.
- [27] V. Verma, Optimization of parameters affecting the performance of passive solar distillation system by using Taguchi method, *IOSR J. Mech. Civ. Eng.*, 7 (2013) 37–42.
- [28] W.M. El-maghlany, An approach to optimization of double slope solar still geometry for maximum collected solar energy, *Alexandria Eng. J.*, 54 (2015) 823–828.
- [29] H.A. Begum, M.A. Yousuf, K. Siddique-e Rabbani, Effect of top cover material on productivity of solar distillation unit, *Bangladesh J. Med. Phys.*, 9 (2018) 11–16.
- [30] H.R. Goshayeshi, M.R. Safaei, Effect of absorber plate surface shape and glass cover inclination angle on the performance of a passive solar still, *Int. J. Numer. Methods Heat Fluid Flow*, 30 (2020) 3183–3198.
- [31] F. Banat, R. Jumah, M. Garaibeh, Exploitation of solar energy collected by solar stills for desalination by membrane distillation, *Renewable Energy*, 25 (2002) 293–305.
- [32] B.A. Akash, M.S. Mohsen, W. Nayfeh, Experimental study of the basin type solar still under local climate conditions, *Energy Convers. Manage.*, 41 (2000) 883–890.
- [33] M.Z. Malik, F. Musharavati, S. Khanmohammadi, S. Khanmohammadi, D.D. Nguyen, Solar still desalination system equipped with paraffin as phase change material: exergoeconomic analysis and multi-objective optimization, *Environ. Sci. Pollut. Res.*, 28 (2021) 220–234.
- [34] M. Khan, M. Mustafa, Solar still distillate productivity enhancement by using reflector and design optimization, *Innov. Energy Res.*, 8 (2019) 1–10.
- [35] A.E. Kabeel, Z.M. Omara, F.A. Essa, Improving the performance of solar still by using nanofluids and providing vacuum, *Energy Convers. Manage.*, 86 (2014) 268–274.
- [36] D. Dsilva Winfred Rufuss, S. Iniyani, L. Suganthi, P.A. Davies, T. Akinaga, Analysis of Solar Still with nanoparticle Incorporated Phase Change Material for Solar Desalination Application, *Solar World Congress 2015/ISES Conference Proceedings*, Daegu, Korea, 8–12 November 2015, 2015, pp. 1271–1280.
- [37] B. Gupta, P. Shankar, R. Sharma, P. Baredar, Performance enhancement using nano particles in modified passive solar still, *Procedia Technol.*, 25 (2016) 1209–1216.
- [38] A.E. Kabeel, Z.M. Omara, F.A. Essa, A.S. Abdullah, T. Arunkumar, Augmentation of a solar still distillate yield via absorber plate coated with black nanoparticles, *Alexandria Eng. J.*, 56 (2017) 433–438.
- [39] O. Mahian, A. Kianifar, S.Z. Heris, D. Wen, A.Z. Sahin, S. Wongwises, Nanofluids effects on the evaporation rate in a solar still equipped with a heat exchanger, *Nano Energy*, 36 (2017) 134–155.
- [40] S. Rashidi, M. Bovand, N. Rahbar, J. Abolfazli, Steps optimization and productivity enhancement in a nano fluid cascade solar still, *Renewable Energy*, 118 (2018) 536–545.
- [41] M.R. Safaei, H.R. Goshayeshi, I. Chaer, Solar still efficiency enhancement by using graphene oxide/paraffin nano-PCM, *Energies*, 12 (2019) 2002, doi: 10.3390/en12102002.
- [42] G.B. Balachandran, P.W. David, R.K. Mariappan, A.E. Kabeel, M.M. Athikesavan, R. Sathyamurthy, Improving the efficiency of single-sloped solar still using thermally conductive nanoferric oxide, *Environ. Sci. Pollut. Res.*, 27 (2020) 32191–32204.
- [43] K.M. Bataineh, M. Abu Abbas, Improving the performance of solar still by using nanofluids, vacuuming, and optimal basin water thickness, *Desal. Water Treat.*, 173 (2020) 105–116.
- [44] M. Tarawneh, P.V.R. Sethupathi, P. Senthil, Parametric optimization for improving the performance of single slope solar still through experimental studies, *Int. J. Eng. Sci. Res. Technol.*, 5 (2016) 291–299.
- [45] S. Verma, D. Singh, A.K. Sharma, Experimental investigations on a single slope solar still, *Int. Res. J. Eng. Technol.*, 5 (2018) 2658–2662.
- [46] R. Balaji, V. Aravindh, J. Baburangan, S. Koushik, P. Mahendran, Performance analysis of single slope solar still using sensible heat storage material, *Appl. Innov. Res.*, 1 (2019) 120–127.
- [47] A.A. Fatani, G.M. Zaki, A. Al-Turki, Improving the yield of simple basin solar stills as assisted by passively cooled condensers, *Renewable Energy*, 4 (1994) 377–386.
- [48] M. Jobrane, A. Kharroubi, A. Kahn, A. Kopmeier, C. Penny, Theoretical investigation of a novel solar still configuration for enhanced high-quality drinking water production, *WIT Trans. Ecol. Environ.*, 239 (2019) 181–192.
- [49] Z.A.K. Baharin, M.F. Asmi, N.R.N. Masdek, Effect of cone shape condenser plate tilt angle on solar still productivity, *IOP Conf. Ser.: Earth Environ. Sci.*, 2nd International Conference on Green Environmental Engineering and Technology 23–24 July 2020, Seoul, South Korea, 616 (2020) 012038.
- [50] M.O. Abu Abbas, M.Y. Al-Abed Allah, Q.N. Al-Oweiti, Optimization analysis of active solar still using design of experiment method, *Drinking Water Eng. Sci. Discuss.*, (2020) 1–24, doi: 10.5194/dwes-2020-22.
- [51] A. Ghoneyem, Software to analyze solar stills and an experimental study on the effects of the cover, *Desalination*, 114 (1997) 37–44.
- [52] M. Boukar, A. Harmim, Effect of climatic conditions on the performance of a simple basin solar still: a comparative study, *Desalination*, 137 (2001) 15–22.
- [53] D. Kumar, A. Layek, A. Kumar, Performance enhancement of single slope solar still integrated with flat plate collector for different basin water depth, *AIP Conf. Proc.*, 2273 (2020) 050007, doi: 10.1063/5.0024247.
- [54] B.A.K. Abu-Hijleh, H.M. Rababa'h, Experimental study of a solar still with sponge cubes in basin, *Energy Convers. Manage.*, 44 (2003) 1411–1418.
- [55] P. Meukam, D. Njomo, A. Gbane, S. Toure, Experimental optimization of a solar still: application to alcohol distillation, *Chem. Eng. Process. Process Intensif.*, 43 (2004) 1569–1577.
- [56] H.S. Aybar, Mathematical modeling of an inclined solar water distillation system, *Desalination*, 190 (2006) 63–70.
- [57] P.K. Abdenacer, S. Nafila, Impact of temperature difference (water-solar collector) on solar-still global efficiency, *Desalination*, 209 (2007) 298–305.
- [58] F. Ullah, M. Kang, Performance evaluation of parabolic trough solar collector with solar tracking tilt sensor for water distillation, *Energy Environ.*, 30 (2019) 1219–1235.
- [59] H. Al-Hinai, M.S. Al-Nassri, B.A. Jubran, Effect of climatic, design and operational parameters on the yield of a simple solar still, *Energy Convers. Manage.*, 43 (2002) 1639–1650.
- [60] M.Z. Khan, J.M. Islamia, J. Nagar, Optimization of single slope solar still geometry for maximum collected solar radiation, *Adv. Phys. Theor. Appl.*, 57 (2016) 45–50.

- [61] T. Mohammadi, M.A. Safavi, Application of Taguchi method in optimization of desalination by vacuum membrane distillation, *Desalination*, 249 (2009) 83–89.
- [62] S.J.P. Gnanaraj, S. Ramachandran, Optimization on performance of single-slope solar still linked solar pond via Taguchi method, *Desal. Water Treat.*, 80 (2017) 27–40.
- [63] K. Zarzoum, K. Zhani, H.B. Bacha, Experimental validation of optimized solar still using solar energy, *J. Fundam. Renewable Energy Appl.*, 7 (2017).
- [64] A.M. Ahmed, A.H. Ahmed, R.W. Daoud, O.K. Ahmed, Optimization of Simple Solar Still Performance Using Fuzzy Logic Control, 2020 6th International Engineering Conference "Sustainable Technology and Development" (IEC), 2020, pp. 205–210.
- [65] A. Bagheri, N. Esfandiari, B. Honarvar, A. Azdarpour, ANN modeling and experimental study of the effect of various factors on solar desalination, *J. Water Supply Res. Technol. AQUA*, 70 (2021) 41–57.
- [66] S. Jafari, M. Aghel, A. Sohani, S. Hoseinzadeh, Geographical preference for installation of solar still water desalination technologies in Iran: an analytical hierarchy process (AHP)-based answer, *Water (Switzerland)*, 14 (2022) 265, doi: 10.3390/w14020265.
- [67] Y. Zhao, O. Ramadan, H. Kong, X. Xue, S. Riffat, H. Zheng, Performance analysis and optimization of a novel high-efficiency flower-inspired solar still, *Energy Convers. Manage.*, 251 (2022) 114878, doi: 10.1016/j.enconman.2021.114878.
- [68] S.J. Patrick, M.G.L. Annaamalai, Enhancing solar still productivity by optimizing operational parameters, *Desal. Water Treat.*, 254 (2022) 1–14.
- [69] R. Dev, G.N. Tiwari, Characteristic equation of a passive solar still, *Desalination*, 245 (2009) 246–265.
- [70] A.H. Elsheikh, S.W. Sharshir, A.E. Kabeel, R. Sathyamurthy, Application of Taguchi method to determine the optimal water depth and glass cooling rate in solar stills, *Int. J. Sci. Technol.*, 28 (2021) 731–742.
- [71] H.S. Walter Benenson, J.W. Harris, H. Lutz, *Handbook of Physics*, Springer Science & Business Media, Berlin/Heidelberg, Germany, 1959.
- [72] J.M.C. Yunus, A. Çengel, *Fluid Mechanics*, McGraw-Hill Series in Mechanical Engineering, McGraw-Hill Series in Mechanical Engineering, New York, 2014.
- [73] J. Buongiorno, Convective transport in nanofluids, *J. Heat Transfer*, 128 (2006) 240–250.
- [74] S.J. Palm, G. Roy, C.T. Nguyen, Heat transfer enhancement with the use of nanofluids in radial flow cooling systems considering temperature-dependent properties, *Appl. Therm. Eng.*, 26 (2006) 2209–2218.
- [75] R. Ben Mansour, N. Galanis, C.T. Nguyen, Effect of uncertainties in physical properties on forced convection heat transfer with nanofluids, *Appl. Therm. Eng.*, 27 (2007) 240–249.
- [76] R.L. Hamilton, Thermal conductivity of heterogeneous two-component systems, *Ind. Eng. Chem. Fundam.*, 1 (1962) 187–191.
- [77] X.Q. Wang, A.S. Mujumdar, A review on nanofluids – Part I: theoretical and numerical investigations, *Braz. J. Chem. Eng.*, 25 (2008) 613–630.
- [78] A. Kubiacyk, *Evaluation of Uncertainty in Measurements, Student's Guide*, Faculty of Physics, Warsaw University of Technology – Physics Laboratory, 2017.
- [79] R.A. Fisher, *Statistical Methods for Research Workers*, Oliver and Boyd, London, U.K., 1926.
- [80] D. Julong, Introduction to grey systems theory, *J. Grey Syst.*, 68 (1989) 1–24.
- [81] C.-F. Jeffrey Kuo, T.-L. Su, P.-R. Jhang, C.-Y. Huang, C.-H. Chiu, Using the Taguchi method and grey relational analysis to optimize the flat-plate collector process with multiple quality characteristics in solar energy collector manufacturing, *Energy*, 36 (2011) 3554–3562.